Estimating COVID-19 cases and deaths prevented by non-pharmaceutical interventions in 2020-2021, and the impact of individual actions: a retrospective model-based analysis

Kathyrn R Fair[1,*], Vadim A Karatayev[1], Madhur Anand[1], Chris T Bauch[2]

1 School of Environmental Sciences, University of Guelph, Guelph, ON, Canada, N1G 2W1

2 Department of Applied Mathematics, University of Waterloo, Waterloo, ON, Canada, N2L 3G1

*kafair@uoguelph.ca

Abstract

Simulation models from the early COVID-19 pandemic highlighted the urgency of applying non-pharmaceutical interventions (NPIs), but had limited empirical data. Here we use data from 2020-2021 to retrospectively model the impact of NPIs. Our model represents age groups and census divisions in Ontario, Canada, and is parameterised with epidemiological, testing, demographic, travel, and mobility data. The model captures how individuals adopt NPIs in response to reported cases. Combined school/workplace closure and individual NPI adoption reduced the number of deaths in the best-case scenario for the case fatality rate (CFR) from 174,411 [CI: 168,022, 180,644] to 3,383 [CI: 3,295, 3,483] in the Spring 2020 wave. In the Fall 2020/Winter 2021 wave, the introduction of NPIs in workplaces/schools reduced the number of deaths from 17,291 [CI: 16,268, 18,379] to 4,167 [CI: 4,117, 4,217]. Deaths were several times higher in the worst-case CFR scenario. Each additional $7-11$ (resp. $285-452$) individuals who adopted NPIs in the first wave prevented one additional infection (resp., death). Our results show that the adoption of NPIs prevented a public health catastrophe.

Introduction

Non-pharmaceutical interventions (NPIs) such as school and workplace closure, limiting group sizes in gatherings, hand-washing, mask use, physical distancing, and other measures are essential for pandemic mitigation in the absence of a vaccine [1]. Scalable NPIs, in particular, are measures that can be taken up by the entire population in case containment strategies have

failed [2]. These measures have been applied extensively during the 2019 coronavirus disease (COVID-19) pandemic in order to reduce severe outcomes [3]. Given the extensive social and economic consequences of the COVID-19 pandemic, there is significant value in assessing how many cases, hospitalizations, and deaths were prevented by pandemic mitigation measures that relied upon scalable NPIs.

Assessments of the effectiveness of NPIs sometimes rely upon comparing health outcomes in countries that did not implement certain NPIs, to those that did [4]. However, it may be difficult to control for confounding factors in cross-country comparisons such as differing social and economic circumstances. Another approach is to monitor outcomes longitudinally in a given population as they respond to a timeline of changing NPIs [5].

However, empirical approaches to predicting the number of COVID-19 cases in the absence of interventions are difficult or impossible since, in every country, governments implemented control measures and/or the population responded to the presence of the virus. Even in the case of Sweden, whose government famously adopted a *de facto* herd immunity strategy [6], the population exhibited enormous reductions in mobility in March and April 2020 (27%, 61%, and 82% reduced time spent at retail/recreation destinations, transit stations, and workplaces, respectively, at their maximal values) [7]. However, simulation models can be useful the task of estimating the number of cases in the absence of interventions, as well as many other questions concerning SARS-CoV-2 transmission and COVID-19 disease burden [8–18]. Simulation models that were developed early during the pandemic made projections for such scenarios, but required rational assumptions about crucial parameter values in the absence of empirical data specific to COVID-19 [9, 16, 18].

Here we adopt a retrospective approach of fitting a simulation model to empirical data from March 2020 to February 2021 in order to estimate how many COVID-19 cases and deaths would have occurred in the province of Ontario, Canada in the absence of NPIs. After fitting the model to empirical data, we relaxed the parameters relating to NPIs to predict what might have happened in their absence, or in the presence of only a selection of certain NPIs. The model includes the census area and age structure of Ontario, as well as travel between census areas. Moreover, the model accounts for population behavioural responses to pandemic waves: without volitional population uptake of NPIs, "flattening the curve" may not have been possible [17].

Results

Model overview

To capture the social-epidemiological dynamics of severe acute respiratory syndrome coronavirus 2 (SARS-CoV-2) transmission and COVID-19 cases, we developed a stochastic compartmental model incorporating age and spatial structure (Figure 1). Transmission dynamics in the population of each census region are described by a Susceptible (S), Exposed (E), Pre-symptomatic and infectious (P), Symptomatic and infectious (I), Asymptomatic and infectious (A), Removed (R) natural history. Populations in different regions are connected through commuter travel. Transmission is reduced through school and/or workplace closure and infection control efforts in those settings, under direction from public health authorities. However, transmission is also reduced outside of school and work settings as a result of volitional efforts by individuals to adopt NPIs, including measures such as physical distancing, hand-washing, and mask wearing (Supplementary information, Figure S1). This occurs in proportion to the daily incidence of reported cases. Transmission rates are region-specific to account for regional differences in contact patterns due to population density and other factors, and were also modified by seasonality in transmission. Age classes varies in their relative susceptibility. Age-specific testing rates increase over time from initially low levels in March 2020 to a constant level (with the date this is attained varying by age class).

Using Ontario data, we estimated deaths resulting from COVID-19 under best-case and worst-case scenarios for the crude case fatality ratio (CFR). In the best-case scenario we assume that CFR computed from the historical for the first and second waves also applies in counterfactual scenarios where the case incidence was much higher due to relaxing NPIs. In the worst case, we extrapolate the observed empirical relationship between case incidence and CFR to consider the possibility that the CFR increases with case numbers [19], due to increased strain on the healthcare system [20] (Supplementary information, Figure S2).

Epidemiological [21–23], testing [21–23], demographic [24], travel [25], and mobility data [7] for Ontario were used to parameterise the model. We employed a 2-stage non-linear optimization process to fit cases by age class at the provincial level, and total cases at the Public Health Unit (PHU) level [26–28]. The first stage used a global algorithm, with the results of that fitting input as the initial values for the second-stage local optimization. This allowed us to estimate the baseline transmission rate, as well as how it responded to school/workplace closure, and how many individuals adhered to NPIs in response to reported case incidence. Full

details on the model structure and parameterisation appear in the Methods.

Scenarios and outcomes analyzed

We generated model outputs for reported COVID-19 cases and deaths over three time periods. The first time period covers the first wave from 10 March 2020 to 15 August 2020. The second time period from 12 June 2020 to Feb 28 2021 covers Ontario's reopening during the first wave and the subsequent second wave. These periods are studied separately because the first and second waves differed considerably in terms of their epidemiology, disease burden, and interventions. These two time periods were analyzed retrospectively: the empirical data from these time periods were used to fit the model.

In the first time period, Ontario implemented school and workplace closure, and a significant proportion of the population adhered to recommended NPIs. For the first wave, we projected what might have happened under three counterfactual scenarios: (1) school/workplace closures were enacted but no individuals adhered to any other NPIs, (2) school/workplace closures were not enacted but individuals adhered to other NPIs in proportion to reported case incidence, and (3) school/workplace closures were not enacted and no individuals adhered to NPIs (a "do nothing" scenario).

In the second time period, Ontario closed schools and workplaces in late 2020/early 2021, and began re-opening in February 2021, but with mandatory NPIs in place to combat transmission, such as requiring mask use in schools. We considered two counterfactual scenarios for the re-opening phase in February 2021: (1) reopening does not occur (school/workplace closures continues indefinitely), and (2) schools and workplaces are reopened without NPIs in place. Individual NPI adherence varied in response to cases in homes and other locations for all of these scenarios. We also note that all of our scenarios for the second time period incorporated the first provincial imposition of control measures in Spring 2020 followed by the first provincial re-opening in Summer 2020.

For the first time period and with reference to the average population uptake of NPIs during those periods, we also estimated how many additional individuals must adopt NPIs in order to prevent one additional case, or one additional death (i.e., incremental cases and death prevented by NPI uptake). These measures gauge the impact of individual-level efforts on the course of the pandemic. The numbers are calculated as an incremental quantity because the incremental effectiveness of an individual choosing to adopt NPIs depends upon how many other individuals

in the population are already doing so, on account of their impact on community transmission.

Cases and deaths prevented by NPIs in the first and second waves

Results for our three counter-factual scenarios in the first wave highlight the key role that NPIs played in limiting the spread of SARS-CoV-2, and also show how school/workplace closures interact with individual-level behaviours concerning NPIs (Figure 2). The actual number of daily reported cases peaked at 640 in Ontario in April 2020, and the modelled time series of cases follows the empirical epidemic curve (Figure 2a, inset). However, in the absence of both school/workplace closure and individual uptake of NPIs, the model predicts that daily number of reported cases would have peaked at 65,000 in May 2020. Allowing for either school/workplace closure or individual uptake of NPIs reduces this peak considerably, although the peaks are still large compared to the factual (historical) scenario where both were applied.

Under the best case scenario for the CFR, the first wave would have resulted in $174,411$ [CI:$168,022,\ 180,644$] deaths in the absence of both school/workplace closure and individual adherence to NPIs (Figure 2b). This number greatly exceeds the $3,383$ deaths that actually occurred between 10 March and 15 August 2020 due to lockdown and population adoption of NPIs [29]. The worst-case scenario for deaths is even higher under the "do nothing" scenario (Figure 2c), on account of the unmanageable surge in cases causing a heightened CFR. However, applying either school/workplace closure or individual uptake of NPIs significantly reduces the number of deaths in both worst- and best-case scenarios. The reductions are greater for applying only individual-level NPI measures than for applying school/workplace closure. This is because school/workplace closure in our model only affects school-age children and working-age adults working in non-essential businesses, whereas individual adoption of NPIs in our model spans all employment sectors in all age groups.

These findings are qualitatively unchanged for the second wave, except that the difference in cases and deaths across the scenarios is not as large, since we did not evaluate a "do nothing" scenario. (Figure 3). As before, cases and deaths are considerably higher when NPI use is limited (in this case, does not occur in workplaces/schools). Both the empirical epidemic curve and the modelled epidemic curves share the feature of a relatively slow rise to a peak, followed by a relatively rapid drop afterwards (Figure 2a). This is due to the combined effect of timing of school/workplace closure, behavioural response, and seasonality in the transmission rate.

Impact of individual-level efforts

We estimated how many additional individuals must adopt NPIs in order to prevent one additional case, and one additional death, given what percentage of the population is already adherent to NPIs. We estimated this under both best-case and worst-case scenarios for the CFR. When the percentage of the population already adherent to NPIs in within empirically valid ranges for the first wave (shaded regions in Figure 4), we estimated that every 7 to 11 individuals who adopted NPIs prevented a single SARS-CoV-2 infection. Similarly, every 285 to 452 (respectively, 159 to 280) individuals who adopted NPIs prevented a single COVID-19 death in the best-case (respectively, worst-case) scenarios.

In the extreme case where a very high percentage of the population is already adherent to NPIs, the incremental number of individuals who must adhere to NPIs to prevent one case or death increases dramatically. This is expected, since high uptake of NPIs can reduce case incidence to very low levels, and thus reduce the incremental benefit of a few more individuals adopting NPIs. Similarly, in the other extreme when few individuals in the population have adopted NPIs, the incremental benefit of each additional individual who adopts NPIs is higher.

Discussion

This suite of simulations informs a picture of how NPIs–particularly the combination of government mandated measures such as school/workplace closure and volitional individual level actions such as physical distancing and hand-washing–strongly mitigated COVID-19 cases and deaths across both age and census area in Ontario. School/workplace closure or individual-level NPIs implemented on their own would also have reduced both cases and deaths considerably, although the absolute numbers would still have been large.

The number of deaths averted by NPIs was particularly large in the first wave. Our projection of $174,411$ deaths in the "do nothing" scenario for interventions and the best-case scenario for the CFR is plausible: supposing that 70% of Ontario's 14.6 million people had been infected in a "do nothing" scenario, the adjusted CFR for Spring 2020 of 1.6% [19] would have resulted in $163,520$ deaths. Moreover, the actual number of deaths would likely have been much higher than suggested by our best-case scenario. The adjusted CFR of 1.6% was estimated from a population where the ICU capacity in Spring 2020 was not greatly exceeded [29]. Therefore, the adjusted CFR would have been much higher in a population contending with a massive

surge in cases.

Our results on the number of individuals who must adopt NPIs to prevent one case or death increased dramatically with the percentage of the population already adhering to NPIs (Figure 4). As a result, an individual in a population where most others have already adopted NPIs has a reduced personal incentive to practice NPIs, since the number of cases (and thus their perceived infection risk) is lowered. This suggests the possibility of a free-rider effect whereby non-mitigators gain the benefits of reduced community spread without contribute to infection control [30], although social norms can curb this effect [31, 32].

Our model made several simplifying assumptions that could influence results and/or limit the conditions under which the model can be used. For instance, as our model describes community spread, we are not explicitly accounting for how transmission within congregate living settings, long-term care homes, etc. can cause case numbers to increase rapidly [29, 33, 34]. As well, our simplification of Ontario's tiered system for NPIs at the level of individual public health units [35] into a single aggregate "open with NPIs in place" state may lead us to over/underestimate cases at the PHU level, if the tier that PHU is in is more/less restrictive than the aggregate state.

It is well known that mathematical models can be used for forecasting purposes, but they can also be valuable for conveying insights, or for aspirational purposes. In the latter case, mathematical models can motivate the uptake of behaviours to avoid the worst-case scenarios scenarios predicted by the model. The prosocial preferences that humans often adopt toward infectious disease control [31, 32] suggest that this use of models can be effective. Early mathematical models developed during the COVID-19 pandemic showed us what might happen if we chose not to mitigate the pandemic. Our retrospective analysis that uses data from the past year confirms that we prevented a very large loss of life by our decision to take action, and that each individual person who chose to adopt NPIs helped prevent both cases and deaths.

Methods

Base model

Our model, modified from [16], captures transmission dynamics for SARS-CoV-2 within Ontario, Canada. Age structure is introduced, with age classes 1-5 respectively represent 0-19 years old, 20-39 years old, 40-59 years old, 60-79 years old, and 80+ years old. The model also

includes mechanisms for testing, individual NPI adherence, and the implementation of closures (of schools and workplaces).

We describe the transmission dynamics according to a $SEPAIR$ disease progression. Individuals are classed according to their epidemiological status; susceptible to infection (S), exposed i.e. infected but not yet infectious (E), pre-symptomatic and infectious (P), asymptomatic i.e. infectious without ever developing symptoms (A), symptomatic and infectious (I), or removed i.e. no longer infectious (R). We also incorporate testing for the virus, with individuals classed as having either a known (K) or unknown (U) infection status. Testing occurs for symptomatic, pre-symptomatic, and symptomatic individuals and the outcome of these tests becomes known with some daily probability.

Ontario's population is distributed across 49 census divisions, hereafter referred to as regions [25]. Within our model, each region contains a population with the same size as the census division it represents. Each day within the simulation begins with every individual within age class i in region j travelling to region k for the day, with some probability $\nu_i m_{jk}$. Individuals who travel to another region experience any transmission events in the region they are visiting. At the end of the day, these individuals return to region j.

The travel matrix, $M = [m_{jk}]$ contains empirical data on the frequency of travel between regions [25]. We use a matrix $M^* = [2m_{jk}]$ as input to our model, since the data collected considers only individuals aged 15 and up who commute from their home to their place of work and thus excludes travel by unemployed individuals and those under age 15, as well as travel undertaken for other reasons (shopping, athletics, social events, etc.). We supplement M^* with age-specific travel rates, assuming that young/old individuals travel less frequently than working-age individuals Individuals in age classes 1,4,5 (ages 0-19, 60+) reduce their travel by a factor of $\nu_i = \nu_0$, with $\nu_i = 0$ for age classes 2,3 (ages 20-39, 40-59).

As 81% of reported COVID-19 cases are mild, we assume infected individuals reduce their travel by a factor $r = 0.19$ [36]. Additionally, individuals who test positive for COVID-19 reduce their travel by a factor $\eta = 0.8$ [18, 37], so the combined reduction in travel for an infected individual in age classes 1,4 or 5 who has tested positive is $(1 - \nu_i)(1 - r)(1 - \eta)$. When a region closes its schools, the rate of travel to that region is reduced by a factor ϵ_s, with a similar reduction, ϵ_w, when its workplaces are closed. When both are closed, the combined reduction in travel is $(1 - \epsilon_s)(1 - \epsilon_w)$. Similarly, if a region has its schools or workplaces open, but with NPIs in place, travel is reduced by a factor of $\delta_s\epsilon_s$ and of $\delta_w\epsilon_w$ respectively. These parameters ($\epsilon_w,\ \epsilon_s, \delta_w, \delta_s$) are explained in further detail below, as they are also used to describe

the efficacy of NPIs in reducing contacts in schools and workplaces.

As noted in [16], there is a risk of overestimating the effect of travel, since we assume that all individuals within an age class have an equal likelihood of travelling to another region on any given day. Within real-world populations, the same individuals will tend to travel consistently (e.g. will travel frequently, to the same region, and interact with the same group of contacts). Despite this, it is preferable to err on the side of over-estimation, as travel can substantially impact spread of SARS-CoV-2 through the importation of the virus to regions with few or no cases.

Each individual, i, has a state, $\{D_i^j, T_i^j\}$ based on their age class, $j \in \{1, 2, 3, 4, 5\}$, epidemiological status, $D_i^j \in \{S_i^j, E_i^j, P_i^j, A_i^j, I_i^j, R_i^j\}$, and testing status, $T_i^j \in \{U_i^j, K_i^j\}$. An individual with age class j, epidemiological status D^j, and either testing status is $\{D_i^j, \cdot\}$, similarly for $\{\cdot, T_i^j\}$. Within region k on day t, $P_{t,k}^{D^j T^j}$ is the number of individuals with age class j and state $\{D_i^j, T_i^j\}$, $P_{t,k}^{DT}$ is the number of individuals across all age classes with state $\{D_i, T_i\}$, and $P_{t,k}$ is the total population size.

Every day, states for individuals with age class j in region k are updated according to the following steps:

1. Exposure: With probability $\lambda_{j,k}(t)$, $\{S^j, \cdot\}$ individuals are exposed to SARS-CoV-2 and shift to $\{E^j, \cdot\}$.

2. Onset of infectious period: With probability $(1 - \pi)\alpha$, $\{E^j, \cdot\}$ individuals become pre-symptomatic and infectious and transition to $\{P^j, \cdot\}$, or alternatively (with probability $\pi\alpha$) become asymptomatic and infectious and transition to $\{A^j, \cdot\}$.

3. Onset of symptoms: With probability σ, individuals in $\{P^j, \cdot\}$ become symptomatic and shift to $\{I^j, \cdot\}$.

4. Testing: With probability τ_{k,I^j}, individuals in $\{I^j, U^j\}$ are tested and shift to $\{I^j, K^j\}$, similarly for τ_{k,P^j} and τ_{k,A^j}.

5. Removal: With probability ρ, individuals in $\{I^j, \cdot\}$ and $\{A^j, \cdot\}$ cease to be infectious and are removed to $\{R^j, \cdot\}$.

During the onset of the infectious period, newly infected individuals are assigned as super-spreaders with probability $s = 0.2$ [38]. Super-spreaders are denoted with the subscript s, while non-super-spreaders are denoted by ns, creating sub-divisions within P^j, A^j and I^j given by

P_s^j, P_{ns}^j, A_s^j, A_{ns}^j, I_s^j, I_{ns}^j. The probability of a super-spreader infecting others is $(1-s)/s$ higher than the probability of a non-super-spreader doing so. Several other factors also impact the infection probability. First, the individuals contacts; both those in schools and workplaces (limited by closures) and those in homes (unaffected by closures). Second; the prevalence of the virus within the population. Third; the effectiveness of closures and individual adherence to NPIs in reducing transmission.

Individuals risk contracting or transmitting SARS-CoV-2 when they interact with others. Four possible locations for interactions are assumed; schools (s), workplaces (w), homes (h), and other (o). For each location, a contact matrix $N^l = [n_{ij}^l]$, where $l \in \{s, w, h, o\}$, contains information on age-stratified contact frequencies. Each n_{ij}^l indicates the relative frequency with which age class i has contacts in age class j, normalized using the the highest total number of contacts (across all locations) for a single age class. Matrices (Supplementary information, Figure S4) are generated by aggregating Canada-specific data from [39]. The 75-80 age class in [39] is used as a proxy for our 80+ age class. When aggregating, we weight the data from each 5-year age class by the proportion of Ontario's population that falls within that age-range [24].

Closures reduce contacts in schools (s), workplaces (w). NPIs introduced to combat SARS-CoV-2 transmission in workplaces and schools as they reopen will also reduce contacts, to a lesser extent. $C_k^l(t)$ controls the measures in place for workplaces ($l = w$) or schools ($l = s$) in region k:

$$C_k^l(t) = \begin{cases} 0 \text{ if } l \text{ are completely open,} \\ \delta_l \epsilon_l \text{ if } l \text{ are open with NPIs in place,} \\ \epsilon_l \text{ if } l \text{ are closed.} \end{cases} \tag{1}$$

Parameters $\epsilon_{w,s}$ represent the efficacy of closures in workplaces, and schools. Additionally, $\delta_{w,s} < 1$ control how effective NPIs in workplaces and schools are, in comparison to a closure.

All remaining contacts are assumed to occur at home (h) or in other locations (o), where contacts may be reduced through individual adherence to NPIs. The maximum efficacy of NPIs in homes is denoted by ϵ_h, similarly for other locations by ϵ_o. In region k, the level of individual adherence to NPIs in these locations, $\chi_k(t)$, is a function of perceived risk [40, 41], based on the prevalence of confirmed cases within the region's population, and of the presence/absence of stay-at-home orders in the region, according to

$$\chi_k(t) = 1 - e^{-\left(\omega(t)\left(P_{t,k}^+ / P_{t,k}\right) + L(t)\right)} \tag{2}$$

where $P_{t,k}^{AK} + P_{t,k}^{IK} = P_{t,k}^{+}$ indicates the number of active confirmed cases in the region and

$$L(t) = \begin{cases} 0 \text{ if no stay-at-home orders,} \\ L_0 \text{ if stay-at-home orders in place,} \end{cases} \tag{3}$$

with L_0 capturing the extent to which stay-at-home orders impact NPI adherence. The risk perception coefficient, $\omega(t)$, changes over time, beginning to decrease during the second wave according to

$$\omega(t) = \begin{cases} \omega_0 \text{ if } t < t_d \\ \omega_0 e^{-\zeta(t-t_d)} \text{ if } t \geq t_d \end{cases} \tag{4}$$

where ω_0 is the base risk perception coefficient, t_d corresponds to August 15, 2020 and ζ controls the decay of $\omega(t)$ over time.

Allowing $\omega(t)$ to change over time captures both the idea that perceived risk changes as new information about SARS-CoV-2 and COVID-19 becomes available, and that, though not explicitly modelled, the accumulating costs (economic, social, etc.) associated with NPI adherence may lead individuals to reduce their level of adherence [42, 43]. Ontario-specific data suggests it is plausible to assume these factors are influencing NPI adherence As time passes, the extent to which mobility in retail and recreation locations [7] (our proxy for NPI adherence) decreases when active cases are high is lessened (Supplementary information, Figure S1), in the absence of stay-at-home orders in one or more PHU (i.e. prior to 14 January 2021). Once stay-at-home orders have been introduced, reductions in mobility for a given level of active cases are larger.

Additionally, we estimate a provincial weighted mean value for $\omega(t)$ (Supplementary information, Figure S1) using Ontario-specific data, which begins to decay around mid-August 2020 (we choose this as 15 August 2020 for simplicity). The increase in the estimated $\omega(t)$ value occurring in late December 2020 (prior to the stay-at-home orders) is likely caused by a combination of changing mobility patterns over the winter holiday period, and the declaration of a province-wide shutdown on 26 December 2020. We emphasize that this is a rough estimate of $\omega(t)$, as there is not a one-to-one relationship between PHU and the regions reported in the mobility data, and include it only to illustrate the assumed trend over time.

Accounting for the effects of closures and individual NPI adherence, the fraction of contacts

in age class j which remain for individuals in age class i at time t in region k is:

$$F_{ij,k}(t) = n_{ij}^{w}\left(1 - C_k^{w}(t)\right) + n_{ij}^{s}\left(1 - C_k^{s}(t)\right) + n_{ij}^{h}\left(1 - \epsilon_h \chi_k(t)\right) + n_{ij}^{o}\left(1 - \epsilon_o \chi_k(t)\right). \tag{5}$$

The transmission probability for non-super-spreaders ($\{P_{ns}, \cdot\}, \{A_{ns}, \cdot\}, \{I_{ns}, \cdot\}$) is $\beta_{D_{ns}} = \beta_0^D$, while for super-spreaders ($\{P_s, \cdot\}, \{A_s, \cdot\}, \{I_s, \cdot\}$) we set $\beta_{D_s} = \beta_0^D(1-s)/s$. Individuals who test positive for COVID-19 reduce their contacts by a fraction η, such that while $f_{T=U} = 1$, $f_{T=K} = 1 - \eta$, where $\eta = 0.8$ [18, 37]. The daily probability of a susceptible individual in age class i becoming infected in region k, stated as 1 less the probability of the individual not becoming infected, is:

$$\lambda_{i,k}(t) = 1 - \prod_{D^j, T^j} \left[1 - F_{ij,k}(t) f_T \beta_{i,k}^{D}(t)\right]^{P_{t,k}^{*D^j T^j}} \tag{6}$$

where $\beta_{i,k}^{D}(t)$ is the probability of an individual in region k with epidemiological state D transmitting SARS-CoV-2 to a susceptible individual in age class i, at time-step t. This probability is:

$$\beta_{i,k}^{D} = \xi_k \gamma_i \beta_0^{D} \left[1 + B\cos\left(\frac{2\pi}{365}(t + \phi)\right)\right] \tag{7}$$

where γ_i is an age-specific susceptibility coefficient, ξ_k is a PHU-specific transmission modifier, and seasonality is controlled by B and ϕ so transmission probability peaks sometime in fall/winter and attains its lowest value in spring/summer [44]. Due to epidemiological data being reported at the PHU level ξ_k values are PHU-specific not region-specific and all regions within the same PHU will have identical ξ_k values. The starred notation in $P_{t,k}^{*D^j T^j}$ indicates the number of individuals with state $\{D^j, T^j\}$ in region k at time t after adjusting for travel.

Based on examination of Ontario-specific data on tests completed per day [22], we assume symptomatic testing probability for individuals in age class i changes over time according to

$$\tau_{I_i}(t) = \begin{cases} \tau_{I_0} \text{ if } t < t_{n=50} \\ \tau_{I_{\max}} - (\tau_{I_{\max}} - \tau_{I_0}) e^{-\psi_i (t - t_{n=50})} \text{ if } t \geq t_{n=50} \end{cases} \tag{8}$$

where we have initial, τ_{I_0}, and maximum $\tau_{I_{\max}}$ testing probabilities that hold across all age classes. For each age class, i, we fit values for the parameter, ψ_i, controlling the rate at which the testing probability increases over time. Age-specific testing rates are assumed, as factors such as targeted testing in long-term care homes and schools, and the severity of symptoms in

different age groups can influence the likelihood that a person of a given age is tested [45–47].

We assume that pre-symptomatic and asymptomatic individuals experience a lower testing probability than symptomatic individuals, as provincial testing guidelines limit asymptomatic testing to high risk individuals and those in groups targeted for testing [45]. We set $\tau_{P_{0_i}} = \tau_{A_{0_i}} = 0 \; \forall \; i$. The testing probability for pre-symptomatic individuals in age class i is:

$$\tau_{P_i}(t) = \begin{cases} 0 \text{ if } t < t_{n=50}, \\ \tau_{P_{\max}} \left(1 - e^{-\psi_i (t - t_{n=50})}\right) \text{ if } t \geq t_{n=50}. \end{cases} \tag{9}$$

Similarly, for asymptomatic individuals we have a testing probability:

$$\tau_{A_i}(t) = \begin{cases} 0 \text{ if } t < t_{n=50}, \\ \tau_{A_{\max}} \left(1 - e^{-\psi_i (t - t_{n=50})}\right) \text{ if } t \geq t_{n=50}. \end{cases} \tag{10}$$

For simplicity we assume $\tau_{P_{\max}} = \tau_{A_{\max}} = \kappa \tau_{I_{\max}}$, where $\kappa \in (0, 1)$ and thus

$$\tau_{P_i}(t) = \tau_{A_i}(t) = \begin{cases} 0 \text{ if } t < t_{n=50} \\ \kappa \tau_{I_{\max}} \left(1 - e^{-\psi_i (t - t_{n=50})}\right) \text{ if } t \geq t_{n=50} \end{cases} \tag{11}$$

To implement key events within simulations, and compare our results to empirical data, we use the day the 50th case was detected in Ontario ($t_{n \geq 50}$), 10 March 2020 [21], as our reference point. All time-steps (days) within simulations are measured in relation to $t_{n \geq 50}$. Ontario declared a state of emergency on 17 March 2020, and we assume no NPI adherence occurred prior to this ($\omega = 0$ for $t - t_{n \geq 50} < 7$). Within the model, the measures (closures, reopeninngs) for each PHU apply to all regions within that PHU.

Schools were closed for March Break as of 14 March 2020 and remained closed for the rest of the 2019-2020 school year. We use 8 September 2020 as our school reopening date. Workplaces were closed on 25 March 2020 and we treat the day the majority of Ontario entered Phase 2 of the reopening plan (12 June 2020) as our workplace reopening date. In both cases, reopenings occur with NPIs in place to combat SARS-CoV-2 transmission. Schools closed for the Winter Break on 21 December 2020. A province-wide shutdown came into effect on 26 December 2020 and was upgraded to a stay-at-home order on 14 January 2021, wherein Ontario's population was required to remain at home except for essential trips. During February/March 2021 these orders began to lift, on 8 February 2021 schools reopened in all PHU except for Toronto, Peel,

and York (where schools reopened on 16 February 2021). On 10 February 2021 workplaces reopened in a small number of PHU (Hastings Prince Edward, Kingston, Frontenac and Lennox & Addington, and Renfrew County). For the majority of PHU, workplaces reopened on 16 February 2021, with York held back until 22 February 2021 and Toronto, Peel, and North Bay - Parry Sound until 8 March 2021. We assume that schools in PHU were closed from 21 December 2020 until their February 2021 reopening dates, and likewise that workplaces were closed from 26 December 2021 until their February/March 2021 reopening dates. Stay-at-home orders were in effect from 14 January 2021 until the day that the workplaces in a PHU reopened in February/March 2021.

All fitting, simulations, analysis, and visualization are performed in Rstudio (Version 1.2.5019) using R (Version 4.0.3) [48, 49]. For each scenario we run 5 simulations using each of the 10 best parameter sets (see Parametrisation for details). To meet minimum time requirements to run the code for the simulations on individual-level efforts using our computing facilities, 10 simulations are run for each of the 10 best parameter sets, for each value of the percentage of the population adhering to NPIs.

Parametrisation

We set $\beta_0^{P,A} = 0.5\beta_0^I$, based on our assumed period of infectiousness and data indicating that 44% of SARS-CoV-2 shedding occurs prior to the onset of symptoms [50]. All parameters not obtained from the literature are estimated by fitting modelled (1) time series of newly confirmed cases in each age class (number of individuals in each age class entering $\{\cdot, K\}$ states each day) to data on daily confirmed cases (by reporting date and age) at the provincial level [21]; (2) time series of PHU-level totals for newly confirmed cases across all age classes (aggregated from the region-level model output) to data on daily confirmed cases (by reporting date) at the PHU level [23]; (3) underascertainment ratio (ratio of total cases to confirmed positive cases) at the provincial level to a empirically estimated underascertainment ratio of 8.76 for the United States [51]; and (4) individual NPI adherence, $\xi_k(t)$, to a real-world proxy - the change in mobility trends for retail and recreational locations [7]. The percent change in mobility for these locations (from baseline) is treated as indicative of the percent adherence to NPIs. All parameters are described in the Supplementary information, Table S1.

We employ a 2-stage fitting process, first using a global non-linear optimization algorithm (Improved Stochastic Ranking Evolution Strategy [27]), and then feeding the results of that

process into a second local optimizer algorithm (Constrained Optimization BY Linear Approximations [28]) to refine the solution. Optimization processes are implemented using the Nloptr package for R [26]. During both stages, the algorithms attempt to minimize the value of a cost function which incorporates all of the fitting criteria outlined above. As our global algorithm is stochastic and thus different runs of the fitting process may result in different solutions, we run the process 1000 times. Parameter distributions for the 10 best parameter sets (i.e. those with the lowest cost function value at the end of the fitting) are shown in Supplementary information, Figure S5, Figure S6, and Figure S7. Output from simulations run using these parameter sets is shown in Supplementary information, Figure S8, Figure S9, and Figure S10.

Case fatality ratio

To estimate deaths resulting from COVID-19, we consider 2 scenarios for the crude case fatality ratio (CFR). For the best-case scenario the CFR is calculated using Ontario-specific data [22] at weekly intervals, with the crude CFR in week t given by

$$(\text{crude CFR})_t = \frac{(\text{Total deaths})_t}{(\text{Total new cases})_{t-2}}. \tag{12}$$

A 2-week lag between new cases and deaths is used based on estimates of the interval between symptom onset and a case being reported in Ontario [21] and of the interval between symptom onset and death and between case reporting and death [19, 52, 53]. Here, we assume that the CFR value in week t holds regardless of the number of new cases.

However, increased strain on the healthcare system [20] may mean that the CFR increases with case numbers [19]. We consider this as an alternative worst-case scenario and fit functions of the form

$$(\text{crude CFR})_t = \delta + \mu\left(1 - e^{\nu(\text{Total new cases})_{t-2}}\right) \tag{13}$$

to the crude CFR values calculated for the best-case scenario, over different periods of time. The base CFR is controlled by δ, the maximum is $\delta + \mu$ and ν controls the rate at which the CFR increases with case numbers. Based on the clustering of weekly CFR values plotted vs. weekly cases at 2-week lag (Supplementary information, Figure S2) we identify 3 time periods (23 March 2020 to 31 May 2020, 1 June 2020 to 16 August 2020, 17 August 2020 to 28 February 2021) during which the relationship between new cases and the CFR appeared distinct. Using these groups of points we fit parameter values for Equation 13. When fitting,

we assume that δ must be no smaller than the lowest calculated CFR value (approx. 0.0025), and that $\delta + \mu \leq 0.2$ based on national-level CFR values [54]. For the 23 March 2020 to 31 May 2020 period we exclude from the fitting 3 points corresponding to weeks early in the pandemic where reporting issues result in unusually high CFR values. Fitted values of (δ, μ, ν) for our 3 time periods are (0.01226, 0.1877, 0.0001832), (0.002500 0.1975, 0.00008455), and (0.009264, 0.1113, 0.00008747) respectively. Estimated deaths are calculated as

$$(\text{Deaths})_t = (\text{crude CFR})_t(\text{Total new cases})_{t-2}. \tag{14}$$

To evaluate the accuracy of our CFR functions, we apply them to data on cases in the province (Supplementary information, Figure S11) and find a reasonable level of agreement between reported deaths and deaths calculated using Equation 13.

Extension to individual-level NPI adherence

In our base model, Equation 2 captures, at the population level, how the proportion of the population who adhere to NPIs changes in response to case prevalence. Here, we examine NPI adherence at a more granular level. We consider a population where each individual either adheres or does not adhere to NPIs, and does not switch their behaviour during the simulation. We limit this experiment to our first time period (10 March 2020 to 15 August 2020) as over a longer time period we would expect some individuals to change their adherence.

Within this model extension some constant proportion, x, of the population does not adhere to NPIs (with the remaining $1-x$ adhering). This is achieved by adding a third state variable, B_i^j, for NPI adherence, so the state of individual i in age class j is $\{D_i^j, T_i^j, B_i^j\}$. Thus, $B_i^j \in \{C^j, N^j\}$ for individuals who are, respectively, adhering and not adhering to NPIs. Non-adherent individuals are seeded throughout the population, with the number of non-adherent individuals within age class j in region k proportional to the number of individuals within that age class in that region. The seeding of infections within the population allows for both adherent and non-adherent individuals to be amongst those initially infected.

For every interaction between a susceptible individual and an infectious individual there are 4 possibilities for NPI adherence; both parties are adherent (CC), neither party is adherent (NN), the susceptible individual is adherent but the infectious individual is not (CN) and vice versa (NC). When both parties are adherent, the proportion of contacts remaining (replacing

Equation 5) is:

$$F^{CC}_{ij,k}(t) = n^w_{ij}\left(1 - C^w_k(t)\right) + n^s_{ij}\left(1 - C^s_k(t)\right) + n^h_{ij}(1 - \epsilon_h) + n^o_{ij}(1 - \epsilon_o). \tag{15}$$

If neither party is adherent the remaining fraction of contacts for a susceptible individual is:

$$F^{NN}_{ij,k}(t) = n^w_{ij}\left(1 - C^w_k(t)\right) + n^s_{ij}\left(1 - C^s_k(t)\right) + n^h_{ij} + n^o_{ij}, \tag{16}$$

with no reduction in contacts in either of the "home" or "other" locations.

When only one party is adhering to NPIs (CN or NC) the efficacy of NPI adherence in reducing contacts depends on which party is adherent. When only the susceptible is adherent the remaining fraction of contacts is:

$$F^{CN}_{ij,k}(t) = n^w_{ij}\left(1 - C^w_k(t)\right) + n^s_{ij}\left(1 - C^s_k(t)\right) + n^h_{ij}\left(1 - \theta\epsilon_h\right) + n^o_{ij}\left(1 - \theta\epsilon_o\right) \tag{17}$$

while when only the infectious individual is adherent the remaining fraction of contacts is:

$$F^{NC}_{ij,k}(t) = n^w_{ij}\left(1 - C^w_k(t)\right) + n^s_{ij}\left(1 - C^s_k(t)\right) + n^h_{ij}\left(1 - (1-\theta)\epsilon_h\right) + n^o_{ij}\left(1 - (1-\theta)\epsilon_o\right) \tag{18}$$

where $\theta \in [0, 1]$ indicates the relative importance of the susceptible's choice to adhere with NPIs. For simplicity, we assume $\theta = 0.5$ meaning the adherence of the susceptible and infectious individual are equally important and $F^{CN}_{ij,k}(t) = F^{NC}_{ij,k}(t)$.

During the simulation, adherent susceptibles experience an infection probability:

$$\lambda^C_{i,k}(t) = 1 - \left(\prod_{D^j, T^j, C^j} \left[1 - F^{CC}_{ij,k}(t) f_T \beta^D_{i,k}\right]^{P^{*D^j T^j C^j}_{t,k}} \prod_{D^j, T^j, N^j} \left[1 - F^{CN}_{ij,k}(t) f_T \beta^D_{i,k}\right]^{P^{*D^j T^j N^j}_{t,k}} \right) \tag{19}$$

while non-adherent susceptibles experience an infection probability:

$$\lambda^N_{i,k}(t) = 1 - \left(\prod_{D^j, T^j, C^j} \left[1 - F^{NC}_{ij,k}(t) f_T \beta^D_{i,k}\right]^{P^{*D^j T^j C^j}_{t,k}} \prod_{D^j, T^j, N^j} \left[1 - F^{NN}_{ij,k}(t) f_T \beta^D_{i,k}\right]^{P^{*D^j T^j N^j}_{t,k}} \right). \tag{20}$$

Data availability

Data sets required to run simulations are available in a GitHub repository (`https://github.com/k3fair/COVID-19-ON-model`). Data sets generated from our analysis and simulations are available from the corresponding author upon reasonable request. All epidemiological [21–23], testing [21–23], demographic [24], travel [25], and mobility data [7] used to parametrise the model are publicly available online.

Code availability

Code used for parameter fitting and simulations is available in a GitHub repository (`https://github.com/k3fair/COVID-19-ON-model`). Code used for analysis and visualization is available from the corresponding author upon reasonable request.

References

1. Halloran, M. E. *et al.* Modeling targeted layered containment of an influenza pandemic in the United States. *Proceedings of the National Academy of Sciences* **105,** 4639–4644 (2008).

2. Peak, C. M. *et al.* Individual quarantine versus active monitoring of contacts for the mitigation of COVID-19: a modelling study. *The Lancet Infectious Diseases* **20,** 1025–1033 (2020).

3. Hale, T. *et al.* A global panel database of pandemic policies (Oxford COVID-19 Government Response Tracker). *Nature Human Behaviour,* 1–10 (2021).

4. Brauner, J. M. *et al.* Inferring the effectiveness of government interventions against COVID-19. *Science* **371** (2021).

5. Li, Y. *et al.* The temporal association of introducing and lifting non-pharmaceutical interventions with the time-varying reproduction number (R) of SARS-CoV-2: a modelling study across 131 countries. *The Lancet Infectious Diseases* **21,** 193–202 (2021).

6. Claeson, M. & Hanson, S. COVID-19 and the Swedish enigma. *The Lancet* **397,** 259–261 (2021).

7. Google LLC. *Google COVID-19 Community Mobility Reports.* `https://www.google.com/covid19/mobility/` Accessed: March 2, 2021. 2021.

8. Tuite, A. R., Greer, A. L., De Keninck, S. & Fisman, D. N. Risk for COVID-19 resurgence related to duration and effectiveness of physical distancing in Ontario, Canada. *Annals of Internal Medicine* **173,** 675–678 (2020).

9. Tuite, A. R., Fisman, D. N. & Greer, A. L. Mathematical modelling of COVID-19 transmission and mitigation strategies in the population of Ontario, Canada. *CMAJ* **192,** E497–E505 (2020).

10. Moyles, I. R., Heffernan, J. M. & Kong, J. D. Cost and social distancing dynamics in a mathematical model of COVID-19 with application to Ontario, Canada. *Royal Society Open Science* **8,** 201770 (2021).

11. Tang, B. *et al.* De-escalation by reversing the escalation with a stronger synergistic package of contact tracing, quarantine, isolation and personal protection: feasibility of preventing a COVID-19 rebound in Ontario, Canada, as a case study. *Biology* **9,** 100 (2020).

12. Arino, J. & Portet, S. A simple model for COVID-19. *Infectious Disease Modelling* **5,** 309–315 (2020).

13. Abdollahi, E., Haworth-Brockman, M., Keynan, Y., Langley, J. M. & Moghadas, S. M. Simulating the effect of school closure during COVID-19 outbreaks in Ontario, Canada. *BMC medicine* **18,** 1–8 (2020).

14. Magli, A. C., d'Onofrio, A. & Manfredi, P. Deteriorated Covid19 control due to delayed lockdown resulting from strategic interactions between Governments and oppositions. Preprint at `https://doi.org/10.1101/2020.05.26.20112946` (2020).

15. Phillips, B., Anand, M. & Bauch, C. T. Spatial early warning signals of social and epidemiological tipping points in a coupled behaviour-disease network. *Scientific reports* **10,** 1–12 (2020).

16. Karatayev, V. A., Anand, M. & Bauch, C. T. Local lockdowns outperform global lockdown on the far side of the COVID-19 epidemic curve. *Proceedings of the National Academy of Sciences* **117,** 24575–24580 (2020).

17. Jentsch, P. C., Anand, M. & Bauch, C. T. Prioritising COVID-19 vaccination in changing social and epidemiological landscapes: a mathematical modelling study. *The Lancet Infectious Diseases* (2021).

18. Hellewell, J. *et al.* Feasibility of controlling COVID-19 outbreaks by isolation of cases and contacts. *The Lancet Global Health* **8,** e488–e496 (2020).

19. Abdollahi, E., Champredon, D., Langley, J. M., Galvani, A. P. & Moghadas, S. M. Temporal estimates of case-fatality rate for COVID-19 outbreaks in Canada and the United States. *Cmaj* **192,** E666–E670 (2020).

20. Bravata, D. M. *et al.* Association of intensive care unit patient load and demand with mortality rates in US Department of Veterans Affairs hospitals during the COVID-19 pandemic. *JAMA network open* **4,** e2034266–e2034266 (2021).

21. Ontario Agency for Health Protection and Promotion (Public Health Ontario). *Confirmed positive cases of COVID-19 in Ontario.* `https://data.ontario.ca/dataset/confirmed-positive-cases-of-covid-19-in-ontario` Accessed: March 3, 2021. 2021.

22. Ontario Agency for Health Protection and Promotion (Public Health Ontario). *Status of COVID-19 cases in Ontario.* `https://data.ontario.ca/dataset/status-of-covid-19-cases-in-ontario` Accessed: March 4, 2021. 2021.

23. Ontario Agency for Health Protection and Promotion (Public Health Ontario). *Ontario COVID-19 Data Tool: Case trends.* `https://www.publichealthontario.ca/en/data-and-analysis/infectious-disease/covid-19-data-surveillance/covid-19-data-tool?tab=trends` Accessed: March 4, 2021. 2021.

24. Statistics Canada. *Statistics Canada Catalogue no. 98-316-X2016001.* `http://www12.statcan.gc.ca/census-recensement/2016/dp-pd/prof/index.cfm?Lang=E` Accessed: Sept 25, 2020. 2017.

25. Statistics Canada. *2016 census, catalogue no. 98-400-x2016391.* `https://www150.statcan.gc.ca/n1/en/catalogue/98-400-X2016391` Accessed: Sept 1, 2020. 2016.

26. Johnson, S. G. The NLopt nonlinear-optimization package. `http://github.com/stevengj/nlopt`.

27. Runarsson, T. P. & Yao, X. Search biases in constrained evolutionary optimization. *IEEE Transactions on Systems, Man, and Cybernetics, Part C (Applications and Reviews)* **35,** 233–243 (2005).

28. Powell, M. J. in *Advances in optimization and numerical analysis* 51–67 (Springer, 1994).

29. Ontario Agency for Health Protection and Promotion (Public Health Ontario). *COVID-19 (coronavirus) in Ontario.* `https://covid-19.ontario.ca/data/` Accessed: March 3, 2021. 2021.

30. Reluga, T. C. Game theory of social distancing in response to an epidemic. *PLoS Comput Biol* **6,** e1000793 (2010).

31. Oraby, T., Thampi, V. & Bauch, C. T. The influence of social norms on the dynamics of vaccinating behaviour for paediatric infectious diseases. *Proceedings of the Royal Society B: Biological Sciences* **281,** 20133172 (2014).

32. Li, M., Taylor, E. G., Atkins, K. E., Chapman, G. B. & Galvani, A. P. Stimulating influenza vaccination via prosocial motives. *PloS one* **11,** e0159780 (2016).

33. Fisman, D. N., Bogoch, I., Lapointe-Shaw, L., McCready, J. & Tuite, A. R. Risk factors associated with mortality among residents with coronavirus disease 2019 (COVID-19) in long-term care facilities in Ontario, Canada. *JAMA network open* **3,** e2015957–e2015957 (2020).

34. Gardner, W., States, D. & Bagley, N. The coronavirus and the risks to the elderly in long-term care. *Journal of Aging & Social Policy* **32,** 310–315 (2020).

35. Government of Ontario. *COVID-19 response framework: keeping Ontario safe and open.* `https://www.ontario.ca/page/covid-19-response-framework-keeping-ontario-safe-and-open` Accessed: March 25, 2021. 2021.

36. CDC. *Severe Outcomes Among Patients with Coronavirus Disease 2019 (COVID-19) — United States, February 12–March 16, 2020.* `https://www.cdc.gov/mmwr/volumes/69/wr/mm6912e2.htm` Accessed: August 6, 2020. 2020.

37. Soud, F. *et al.* Isolation compliance among university students during a mumps outbreak, Kansas 2006. *Epidemiology & Infection* **137,** 30–37 (2009).

38. Lloyd-Smith, J. O., Schreiber, S. J., Kopp, P. E. & Getz, W. M. Superspreading and the effect of individual variation on disease emergence. *Nature* **438,** 355–359 (2005).

39. Prem, K. *et al.* Projecting contact matrices in 177 geographical regions: an update and comparison with empirical data for the COVID-19 era. Preprint at `https://doi.org/10.1101/2020.07.22.20159772` (2020).

40. Bish, A. & Michie, S. Demographic and attitudinal determinants of protective behaviours during a pandemic: A review. *British journal of health psychology* **15,** 797–824 (2010).

41. Wise, T., Zbozinek, T. D., Michelini, G., Hagan, C. C. & Mobbs, D. Changes in risk perception and self-reported protective behaviour during the first week of the COVID-19 pandemic in the United States. *Royal Society open science* **7,** 200742 (2020).

42. Coroiu, A., Moran, C., Campbell, T. & Geller, A. C. Barriers and facilitators of adherence to social distancing recommendations during COVID-19 among a large international sample of adults. *PloS one* **15,** e0239795 (2020).

43. Crane, M. A., Shermock, K. M., Omer, S. B. & Romley, J. A. Change in reported adherence to nonpharmaceutical interventions during the COVID-19 pandemic, April-November 2020. *JAMA* **325,** 883–885 (2021).

44. Merow, C. & Urban, M. C. Seasonality and uncertainty in global COVID-19 growth rates. *Proceedings of the National Academy of Sciences* **117,** 27456–27464 (2020).

45. Ontario Ministry of Health. *COVID-19 Guidance for the Health Sector: March 5, 2021.* `https://www.health.gov.on.ca/en/pro/programs/publichealth/coronavirus/2019_guidance.aspx` Accessed: March 24, 2021. 2021.

46. Wu, Z. & McGoogan, J. M. Characteristics of and important lessons from the coronavirus disease 2019 (COVID-19) outbreak in China: summary of a report of 72 314 cases from the Chinese Center for Disease Control and Prevention. *Jama* **323,** 1239–1242 (2020).

47. Covid, C. *et al.* Coronavirus disease 2019 in children—United States, february 12–april 2, 2020. *Morbidity and Mortality Weekly Report* **69,** 422 (2020).

48. RStudio Team. *RStudio: Integrated Development Environment for R.* RStudio, PBC. (Boston, MA, 2020). `http://www.rstudio.com/`.

49. R Core Team. *R: A Language and Environment for Statistical Computing.* R Foundation for Statistical Computing (Vienna, Austria, 2020). `https://www.R-project.org/`.

50. He, X. *et al.* Temporal dynamics in viral shedding and transmissibility of COVID-19. *Nature medicine* **26,** 672–675 (2020).

51. Jagodnik, K. M., Ray, F., Giorgi, F. M. & Lachmann, A. Correcting under-reported COVID-19 case numbers. Preprint at `https://doi.org/10.1101/2020.03.14.20036178` (2020).

52. Verity, R. *et al.* Estimates of the severity of coronavirus disease 2019: a model-based analysis. *The Lancet infectious diseases* **20,** 669–677 (2020).

53. Imperial College COVID-19 response team. *Short-term forecasts of COVID-19 deaths in multiple countries.* `https://mrc-ide.github.io/covid19-short-term-forecasts/index.html` Accessed: March 7, 2021. 2021.

54. Johns Hopkins University & Medicine. *Mortality Analyses.* `https://coronavirus.jhu.edu/data/mortality` Accessed: March 25, 2021. 2021.

Acknowledgements

This research was funded by grants from the Ontario Ministry of Colleges and Universities and the Natural Sciences and Engineering Research Council of Canada (NSERC) Alliance program (to M.A. and C.T.B.). Additionally, the research was made possible by the facilities of the Shared Hierarchical Academic Research Computing Network (SHARCNET: `www.sharcnet.ca`) and Compute/Calcul Canada.

Author information

Contributions

C.T.B. and M.A. conceived the study, K.R.F., V.A.K., M.A., and C.T.B. developed the model and methods, K.R.F. and C.T.B. wrote and edited the manuscript, V.A.K. provided comments on the manuscript, V.A.K. and K.R.F. developed simulation code, and K.R.F. performed all simulations and analysis.

Correspondence

Correspondence and material requests should be addressed to Kathyrn R. Fair.

Competing interests

The authors declare no competing interests.

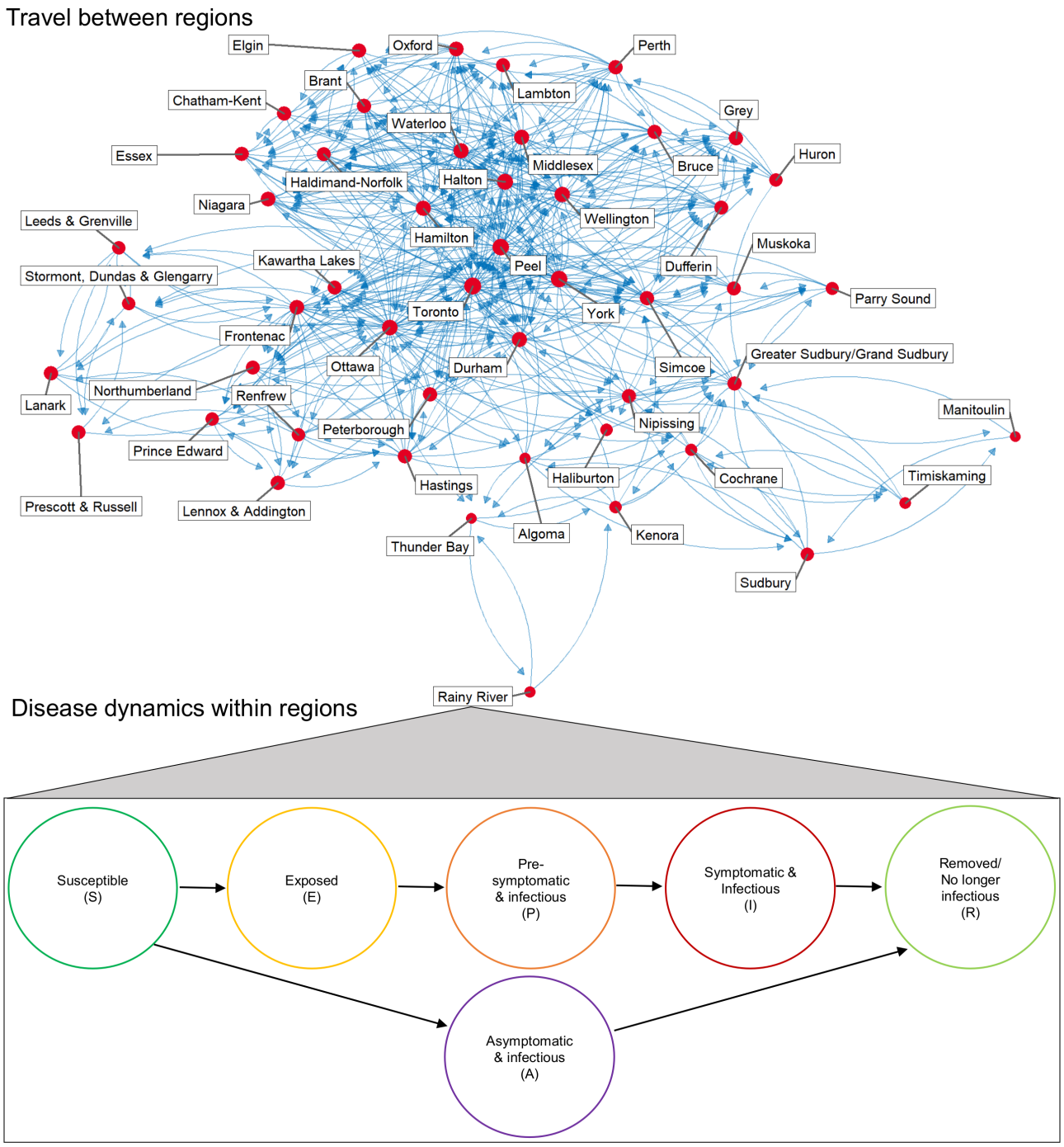

Figure 1. Schematic representation of transmission model. Note that the epidemiological compartments were stratified by age as well as location (see Methods).

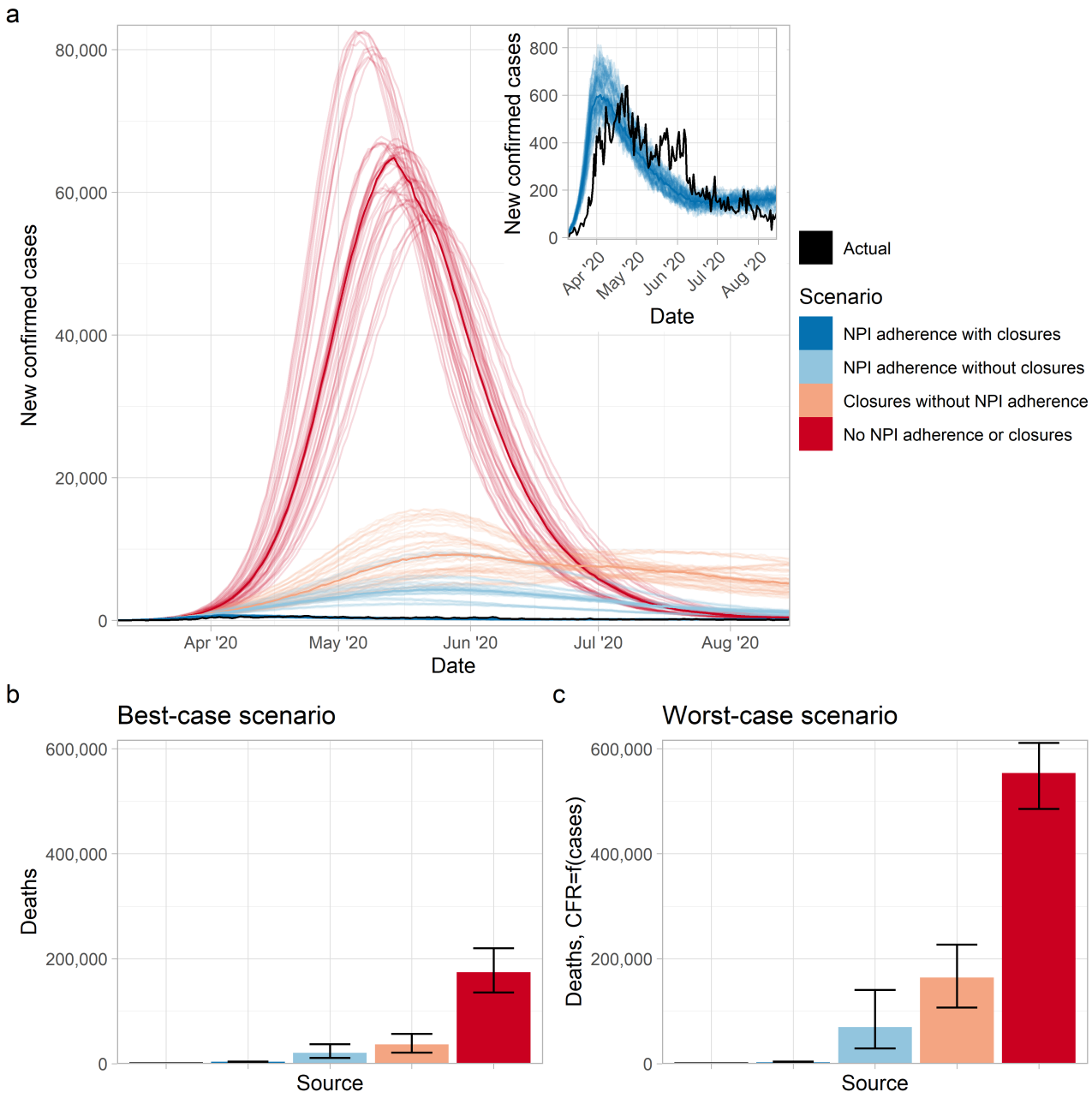

Figure 2. NPIs significantly reduced cases and deaths in the first wave. Figure panels show (a) new confirmed cases by day, and mean projected deaths from 10 March 2020 to 15 August 2020 in (b) the best-case scenario (values from left-right are: 2,789, 3,383, 20,728, 36,782, 174,411) and (c) worst-case scenario (values from left-right are: 2,789, 2,797, 69,590, 164,311, 553,460) for healthcare system functioning in a regime of very high case incidence. Transparent lines in panel (a) correspond to different stochastic realizations of model runs, with solid lines corresponding to the median value across all realizations. Error bars in panels (b,c) represent the minimal and maximal values across all stochastic realizations. Model parameter settings appear in Supplementary information, Table S1.

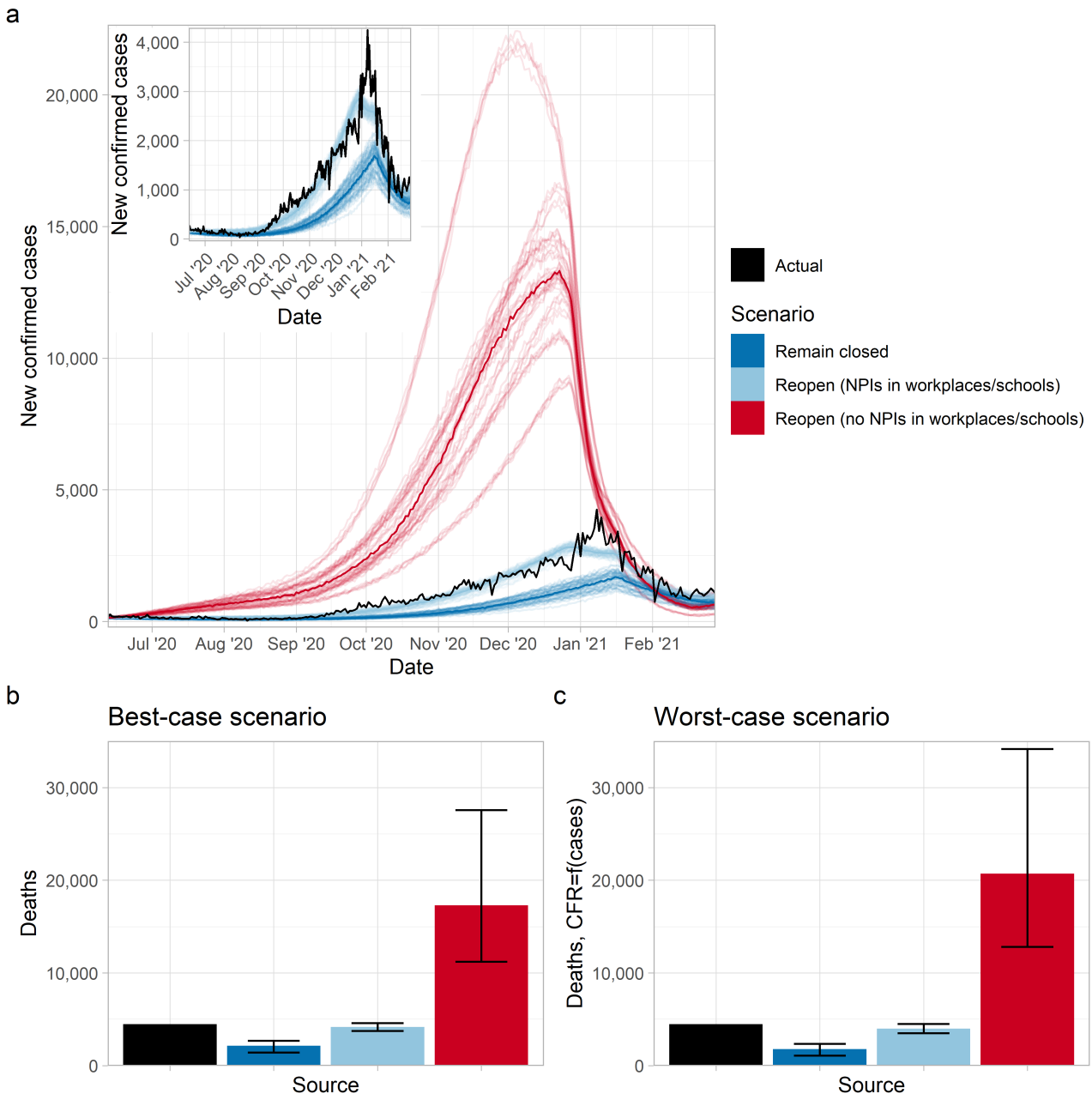

Figure 3. NPIs significantly reduced cases and deaths in the second wave. Figure panels show (a) new confirmed cases by day, and mean projected deaths from 12 June 2020 to 28 February 2021 in (b) the best-case scenario (values from left-right are: $4,493$, $2,154$, $4,167$, $17,291$) and (c) worst-case scenario (values from left-right are: $4,493$, $1,785$, $3,991$, $20,709$) for healthcare system functioning in a regime of very high case incidence. Transparent lines in panel (a) correspond to different stochastic realizations of model runs, with solid lines corresponding to the median value across all realizations. Error bars in panels (b,c) represent the minimal and maximal values across all stochastic realizations. Model parameter settings appear in Supplementary information, Table S1.

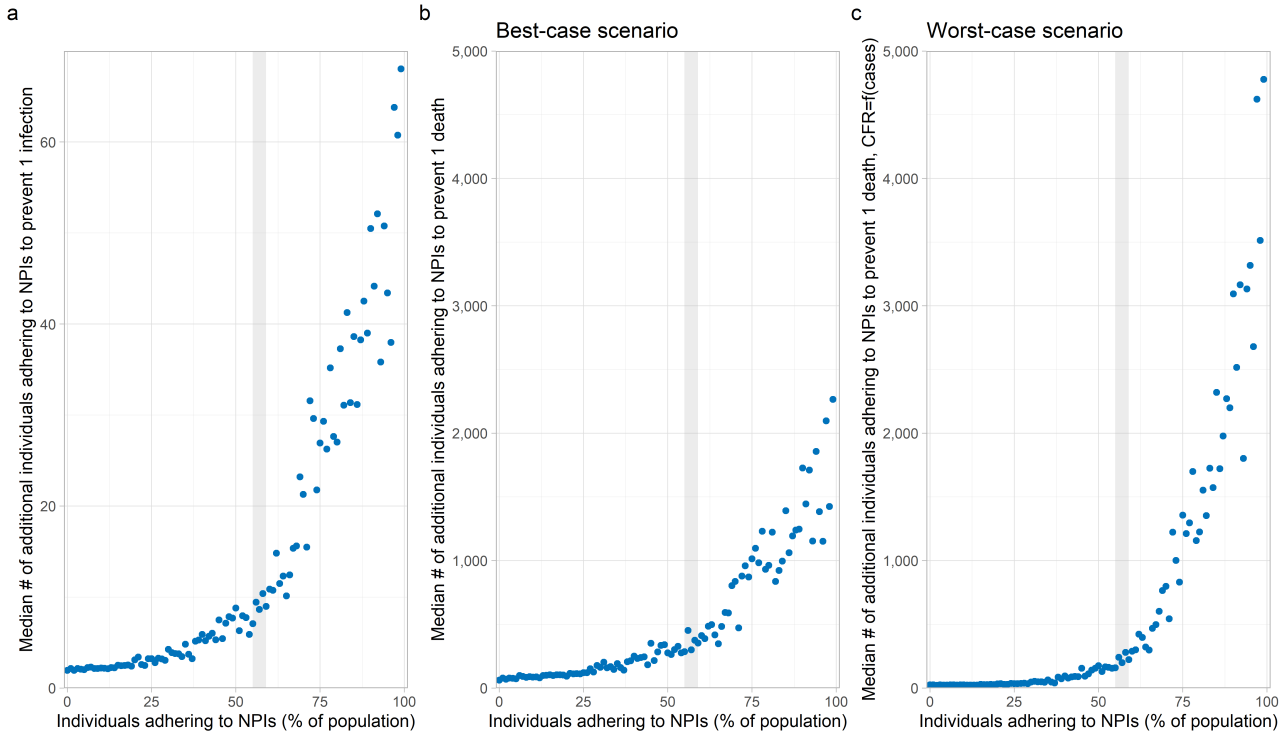

Figure 4. Impact of individual efforts. Figure panels show the incremental median number of individuals who needed to adopt NPIs in order to prevent (a) one infection, and one death under (b) the best-case scenario and (c) worst-case scenario for healthcare system functioning in a regime of very high case incidence, for the first wave (10 March to 15 August 2020). The shaded region demarcates the estimated range in the percentage of individuals adhering to NPIs over that time-period (see Supplementary information, Figure S3). Model parameter settings appear in Supplementary information, Table S1.